crystals

MDPI

Article

Effect of Compact Density of MoO_2 Powders on Densification Kinetics and Grain Growth During Sintering Processes

Jongbeom Lee [1,*], Jaehoon Jung [1,2], Hyowon Lee [3], Jaesoung Park [3] and Haguk Jeong [1]

[1] Industrial Materials Processing R&D Group, Korea Institute of Industrial Technology, Incheon 21999, Republic of Korea; jhjung@kitech.re.kr (J.J.); hgjeong@kitech.re.kr (H.J.)
[2] Department of Advanced Materials Science and Engineering, Inha University, Incheon 22212, Republic of Korea
[3] Thin Film Materials R&D Team, LT Metal. Co., Ltd., Incheon 21697, Republic of Korea; hwlee@ltmetal.co.kr (H.L.); jaspark@ltmetal.co.kr (J.P.)
* Correspondence: ljb01@kitech.re.kr; Tel.: +82-32-850-0378

Abstract: MoO_2 powders compacted under different uniaxial pressures ranging from 100 to 800 MPa, corresponding to the compact densities ranging from 55% to 65%, respectively, were sintered at targeted temperatures within 650–1050 °C for 1 h in an N_2 atmosphere. Then, their densification kinetics and grain growth were investigated. With regard to the densification of MoO_2 powders at room temperature, a linear relationship was observed between the compact density and log pressure in the uniaxial pressure range without fracture and local deformation. The relative densities of the sintered MoO_2 samples increased with increasing compact density and sintering temperature. At a given sintering temperature, the sample with the highest compact density exhibited the best densification rate. The grain size in the sintered samples was proportional to the relative density, and the grain growth obeyed the Arrhenius equation. The sintered samples with 55%, 60%, and 65% densities during the sintering process have different activation energies values depending on the sintering temperature. At low sintering temperatures, the activation energies for 55%, 60%, and 65% compact densities were 50.8, 39.6, and 26.1 kJ/mol, respectively, and at higher sintering temperatures, the corresponding values were 19.8, 21.5, and 25.4 kJ/mol.

Keywords: MoO_2; compact density; sintering; densification; microstructure; grain growth

check for updates

Citation: Lee, J.; Jung, J.; Lee, H.; Park, J.; Jeong, H. Effect of Compact Density of MoO_2 Powders on Densification Kinetics and Grain Growth During Sintering Processes. *Crystals* **2024**, *14*, 1075. https://doi.org/10.3390/cryst14121075

Academic Editors: Karolina Siedliska, Kamila Komędera and Raffaello Mazzaro

Received: 22 November 2024
Revised: 5 December 2024
Accepted: 12 December 2024
Published: 13 December 2024

Copyright: © 2024 by the authors. Licensee MDPI, Basel, Switzerland. This article is an open access article distributed under the terms and conditions of the Creative Commons Attribution (CC BY) license (https://creativecommons.org/licenses/by/4.0/).

1. Introduction

Sintering is a crucial process in the manufacture of ceramic materials as it bonds particles together to attain strong and functional shapes by employing a firing mechanism. The sintering process is irreversible because the particles sacrifice surface energy to build bonds; the reductions in surface energy and interparticle pores via high-temperature atomic diffusion drive sinter bonding. This is typically a high-temperature, time-consuming process, particularly in the case of ceramic materials that exhibit high melting points and low atomic diffusion coefficients [1,2]. Efforts toward the further commercialization of sintered products have manly sought to enhance densification to achieve improved toughness and strength. The densification of ceramic materials depends on several factors such as temperature, time, particle size, distribution, and initial density (or compact density) [3–5].

Powder processing is a common technique used for forming ceramic products before sintering. Ceramic powder pressing is a common green forming technique because of its low cost, high speed, and intermediate shape-forming capability. Furthermore, the quality of the microstructure of a sintered powder compact strongly depends on the density of the green compact, which, in turn, is determined by the behavior of the powder during compaction [6]. During sintering of the ceramic powder compact, densification and grain growth occur simultaneously [7]. Diffusional mechanisms dominate the sintering process under high-temperature conditions, and the dominant path for diffusion is usually along

the grain boundaries [8]. Grain boundary diffusion may govern the sintering process because, from the perspective of the classical grain boundary diffusion theory, the grain boundaries act as perfect sources and sinks for the diffusing species during the diffusion process, and an interface reaction concurrently occurs owing to the addition or removal of vacancies from the grain boundary. Both grain boundary diffusion and interface reactions cause the densification and grain growth of the ceramic powder compact and control the sintering process [9]. As aforementioned, the configuration of interconnected powders differ depending on the powder compact density, and such a network of powders can significantly affect the densification and grain-growth rate because of the limitations of grain boundary diffusion and interface reactions during sintering. However, studies on the densification and grain growth of ceramic powders with different compact densities have been scarce.

For the fine bezel in a thin-film transistor (TFT) backplane, MoO_2 is applicable as a cost-effective and reliable thin-film material. As a functional film, it lowers the reflection of the metal-mesh electrode and enhances shadow elimination [10]. The thin film was fabricated via a sputtering process using a MoO_2 target, and the target was manufactured using a sintering process using MoO_2 powder. The quality of a thin film is influenced by its microstructure, that is, the densification and grain size of the target materials [11–13]. In addition, pressureless sintering (PS) is advantageous in fabricating complicated ceramic components as compared to spark plasma sintering (SPS) or hot pressing (HP), which are associated with restricted sample sizes. However, the comprehensive performance of PS, including high-temperature strength and creep or ablative resistance, is severely limited [14,15]. As the display industry moves towards larger sizes, there is an increasing demand for large-area target materials. While SPS and HP sintering processes require large-scale equipment, leading to exponentially increasing costs, PS offers a cost-effective solution for producing large-area target materials. To enhance the quality of MoO_2 target materials, densification is essential, necessitating research on densification mechanisms, inter-particle diffusion, and grain growth. However, research in this area remains limited.

This study aimed to investigate the solid-state sintering process of pure micro-MoO_2 powders. By studying the kinetics of densification and grain growth in binderless powder compacts of varying densities, we sought to gain insights into the sintering behavior. Given the influence of densification and grain size, investigating grain-growth kinetics can prove theoretical guidance to determine the powder compact density for achieving the desired properties. In addition, a plot of grain size versus relative density was drawn to express the densification and grain growth of MoO_2 compacted powder during sintering.

2. Materials and Methods

Commercial MoO_2 powder (99.9% purity; MTI Corp, Richmond, CA, USA) with polygonal structures and a mean particle size of 1.85 ± 0.7 μm were used as the raw powder. As shown in Figure 1a, the powder exhibited a polygonal morphology. The particle size distribution histogram (Figure 1b) revealed that the particle size distribution was relatively narrow, centered around 1.85 μm, with minor populations at large (approximately 3 μm) and small (approximately 1 μm) particles. The XRD pattern of the powder (Figure 1c) showed peaks at nearly identical 2θ values compared to the COD 96-154-8688 standard for MoO_2 (monoclinic, a = 5.61Å; b = 4.85 Å; c = 5.62 Å; β = 120.9°), indicating a high degree of phase purity with negligible impurities [16]. The powder was weighed and fed into a cylindrical steel die for compression. To minimize friction between the powder and the mold during compaction, the mold surface was coated with zinc stearate. In this study, to investigate the particle diffusion between powders as a function of compact density, powder samples were compacted without any binder and subsequently sintered. The powder was compressed uniaxially at pressures between 100 and 800 MPa into compacts of 6 mm diameter. In each case, the pressure was retained for 5 min to achieve even spreading of pressure. Compact densities of 55–65% were achieved. The compact density was determined using the apparent density method. The apparent density was calculated

by measuring the weight of the compacted sample and determining its volume. The apparent densities measured under the same pressure showed approximately 1% variation. Subsequently, the green compacts were placed in a high-temperature electrical furnace (MTI Corp, Richmond, CA, USA) under N_2 atmosphere. The sintering profile commenced with a heating rate of 5 °C/min up to the targeted sintering temperatures (650–1050 °C). The holding time was 1 h at each designated temperature. The samples were cooled at a rate of 20 °C/min to room temperature. The sintering temperature interval used in the study was 50 °C. To ensure specific temperature control, a type-S thermocouple was applied to the furnace equipment, and the electric power required for the set sintering schedule was traced using a potentiometer. The densities of the green compacts and sintered samples were measured using the geometric method and Archimedes' principle, respectively. A theoretical density value of 6.46 g/cm^3 was calculated on the basis of the X-ray diffraction (Rigaku Smartlab, Rigaku Co., Ltd., Tokyo, Japan) results.

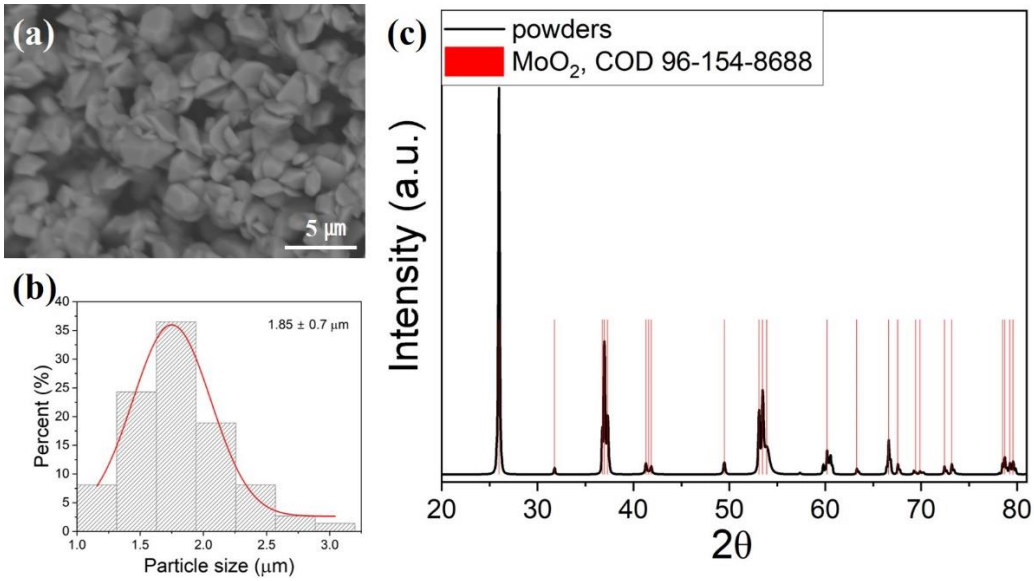


Figure 1. (**a**) SEM image, (**b**) particle size distribution, and (**c**) XRD patterns of the as-received MoO_2 powders.

For scanning electron microscopy (SEM), gold was sputtered on the sample surface to ensure sufficient conductivity. Field-emission scanning electron microscopy (FE-SEM; SU5000, Hitachi Co., Ltd., Tokyo, Japan) was performed at an accelerating voltage of 15 kV to characterize the surface morphology during sintering. The mean grain sizes of the samples prepared under different conditions were statistically measured based on the recorded images and calculated using an image analysis software (Image-Pro v.10.0.13, Media Cybernetics Inc., Rockville, MD, USA). The mean grain size was determined using the following equation [17]:

$$G = 1.56 \times L \quad (1)$$

where G is the mean grain size and L is the mean grain boundary length for approximately 80 grains.

3. Results and Discussion

Figure 2a shows the relationship between the compact density and uniaxial pressure of the MoO_2 powders. Evidently, the compact density of the powders suddenly increased at a low pressure of 100 MPa, and it gradually increased with an increase in applied pressure. In the initial state of compaction under a pressure of 100 MPa, the powder particles were rearranged owing to the filling of large pores, thereby necessitating a low pressure. When the rearrangement of the particles is complete, the powder particles can be packed by forming a localized agglomeration, resulting in a reduction in the volume of the powder

mass with further applied pressure [18]. Figure 2b shows the linear relationship between compact density and log pressure. In contrast to previous reports [19], the results of this study did not exhibit a second linear dependence of the density on the log pressure; the critical stress corresponding to the change in slope was interpreted as a qualitative index of the fracture stress of the particle, leading to continued sliding and rearrangement [20]. Below 800 MPa, the MoO_2 powders completely glided and rearranged without fracturing and local deformation.

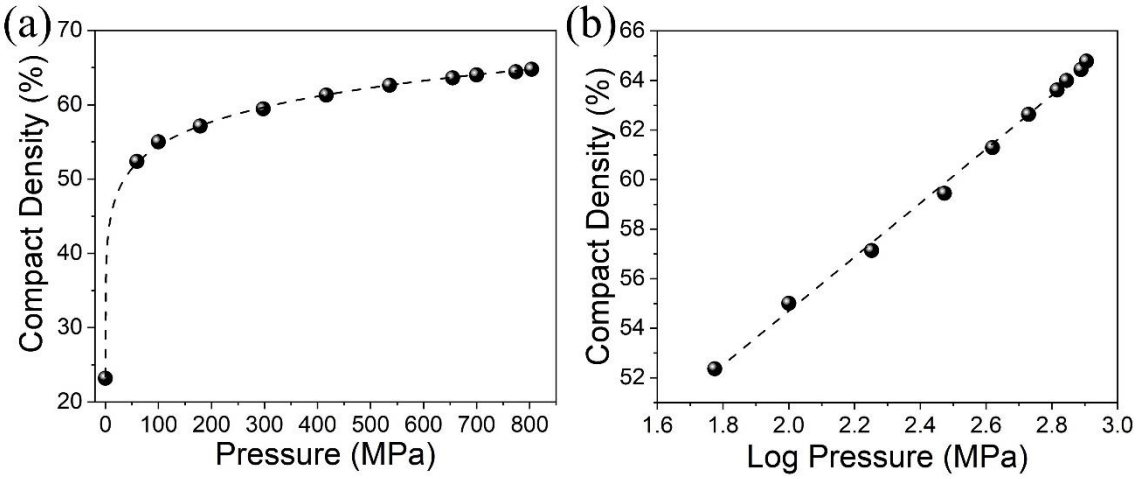


Figure 2. Variation in relative compact density with (**a**) pressure and (**b**) log pressure.

Figure 3a shows the relative densities of the MoO_2 samples sintered at different temperatures. The sintering temperatures are 650–1050 °C at intervals of 50 °C, and the dotted curves were plotted based on the Boltzmann fitting function by using a data analysis software (Origin2023b, Origin Lab, Northampton, MA, USA). The curves exhibit a familiar sigmoidal shape, indicating that the sintered densities obtained at any sintering temperature show a modest but systematic dependence on the compact densities. The maximum density at the sintering temperature of 1050 °C depended on the compact density; the higher the compact density, the greater the sintered density. The sigmoidal shapes in Figure 2a have been reported in several studies on the variation in the relative density with the heating rate for ceramic powders [21,22]. Figure 2b shows the densification rates (K) at different sintering temperatures. The densification rate ($\dot{\rho}$) is widely used to explore densification kinetics and is calculated by using the following equation [23]:

$$\dot{\rho} = \frac{d\rho}{\rho dt} \tag{2}$$

where ρ is the relative density and t is the heating time (s). The heating rate was fixed at 5 degrees Celsius per minute, and the time derivative of density was calculated for each sintering temperature. As shown in the plots in Figure 2b, the densification rate of the sample with a lower compact density remains consistently lower than that of the sample with a higher compact density throughout the entire sintering temperature range of 650–1050 °C. A lower compact density indicates a larger porosity within the sample, and the elimination of the solid/vapor interface is faster than that of the sample with a higher compact density. This is because the surface diffusion from the surface source to the neck of the powder has the lowest activation energy at lower sintering temperatures. Moreover, particle rearrangement is probably more predominant at lower compact densities owing to the much lower rigidity of the particle network. With an increase in the sintering temperature over 650 °C, samples with higher densities exhibit greater densification rates. For atoms to undergo diffusion, they must overcome the energy barrier associated with

changing their position. This necessitates an increase in the kinetic energy of the atoms, requiring a corresponding increase in the temperature based on the following equation:

$$v = v_0 exp\left(\frac{-G^*}{K_B T}\right) \quad (3)$$

where v_0 is the pre-exponential factor, G^* is the magnitude of the energy barrier, K_B is Boltzmann's constant, and T is the temperature. The higher the compact density, the smaller he porosity; therefore, the atoms in a sample with a higher compact density can easily diffuse or jump, thereby enhancing the densification rate. Therefore, a peak densification rate for higher compact density is represented at lower sintering temperatures, as can be seen in Figure 2b.

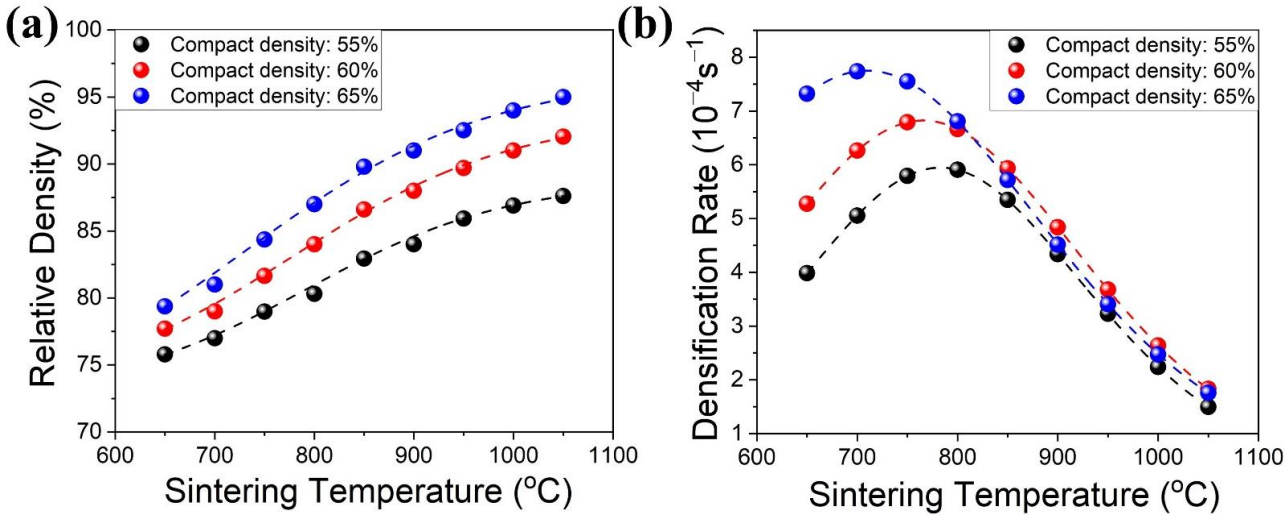


Figure 3. (**a**) Relative densities of MoO_2 samples sintered at different temperatures. (**b**) Plots of densification rate and sintering temperatures.

Figure 4 shows the XRD patterns of as-received MoO_2 powder and MoO_2 samples sintered at different temperatures. The positions of the major and minor peaks in the XRD patterns are nearly identical for all samples, suggesting that no substantial phase transformation occurred in MoO_2 during the sintering process conducted under N_2 atmosphere at temperatures ranging from 650 to 1050 °C for 1 h.

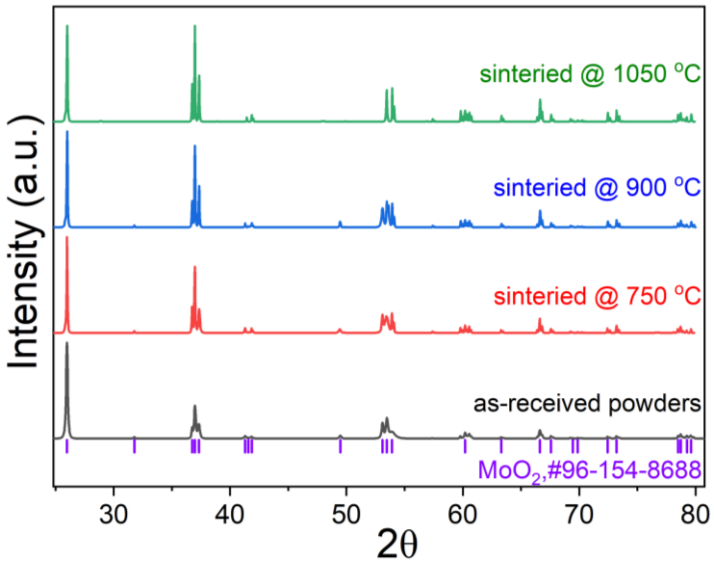


Figure 4. XRD patterns of as-received MoO_2 powders and samples sintered at different temperatures.

Figure 5 shows the microstructures of the fracture cross-section of the sintered samples with different compact densities; the relative densities were less than 0.95. As evident from the images, the microstructure shows loosely packed particles and pores forming an interconnected network through the material. During the sintering process, grain growth of the powders occurred compared with the initial size of 1.85 μm. In addition, the grain sizes of the sintered samples increased with an increase in the compact density. An apparent tendency to evolve toward a more homogeneous microstructure with a higher compact density due to particle rearrangement is noted. Particle rearrangement is geometrically possible because of free-space interparticle forces. At higher compact densities, more interparticle forces are exerted by capillary tension upon sintering, with greater activation of surface diffusion. With an increase in the sintering temperature, coarsening occurs owing to the increase in interparticle contact, which is repeatedly perturbed by surface diffusion and movement of the grain boundary; therefore, more coarsening particles are observed in the sample with the highest compact density (Figure 5c) [23].

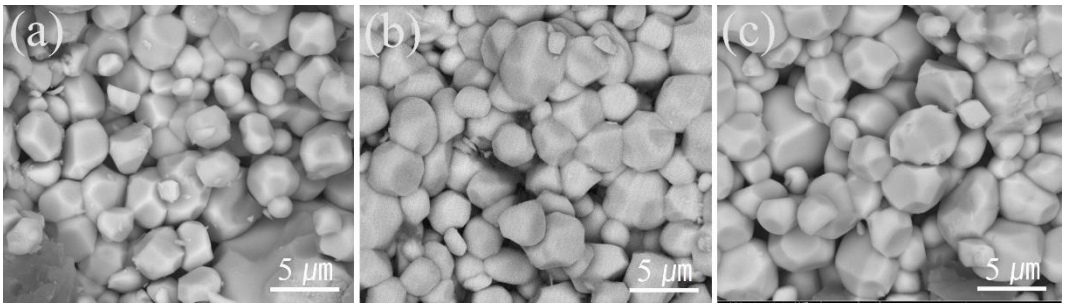


Figure 5. SEM images of the fracture cross-section of the sintered MoO_2 samples with the compact densities of (**a**) 55%, (**b**) 60%, and (**c**) 65% at 1050 °C for 1 h.

Figure 6 shows a plot of the mean grain size versus sintering temperature for varied compact density. As shown in the figures, the mean grain size increased with increasing sintering temperature and compact density, implying a linear relationship between mean grain size and sintering temperature. The dotted lines are fitted by individual points, and the slope value increases with the compact density. The sintering process involves pore elimination via interfacial atomic diffusion, and according to classical sintering theory, this mechanism dominates densification [24]. This can be represented as a particle/pore microstructure as in Figure 3, which is visualized using a random particle network described by DeHoff [25]. The coordination number N of an average particle in this network increases with the density as according to the following equation [26]:

$$\frac{1-\rho}{\rho} = \frac{\pi}{N-2} \tag{4}$$

An increase in N indicates an increase in the contact area between the particles, and the frequency of atoms jumping into neighboring particles also increases. The particles in the samples with a higher compact density easily coarsened at a higher rate. A particle with a tetrakaidecahedron shape, which is a 14-sided polygon with 35 edges and 24 corners that packs to full density, are apparently observed in the sample with a compact density of 65% more than that of 55%.

Figure 7 shows a compilation of the measured grain sizes plotted against the density for all samples with different compact densities. The grain size increased with increasing relative density, and based on the plots, the increasing rate of the grain size can be divided into three stages. Stage 1, below a relative density of approximately 78%, shows rapid grain growth owing to the surface diffusion over a long time at low temperatures, possibly contributing to grain growth without significant densification (Figure 2a) [1]. Below a relative density of 80% in stage 1, such a loose compact state follows Lay's densification model [27] because the particles can rotate easily due to the grain boundary torque, which

provides a large dihedral angle and favorable conditions for grain growth, resulting in rapid grain growth [28]. The slower grain growth in stage 2 was caused by the interconnected pores, which had a strong pinning effect on the grain boundary and restrained grain-boundary movement. However, the densification rate was high because of pore shrinkage and movement through grain boundary channels. Above a relative density of ~90% in stage 3, the few pores remaining on the grain boundaries have a sufficiently low size such that their mobility becomes close to that of the grain boundary, resulting in enhanced grain growth. The mass of the particles can also be easily transferred owing to the extension of the interconnected area among the particles with densification. This phenomenon of rapid grain growth over a high critical relative density has been reported in previous studies [29,30].

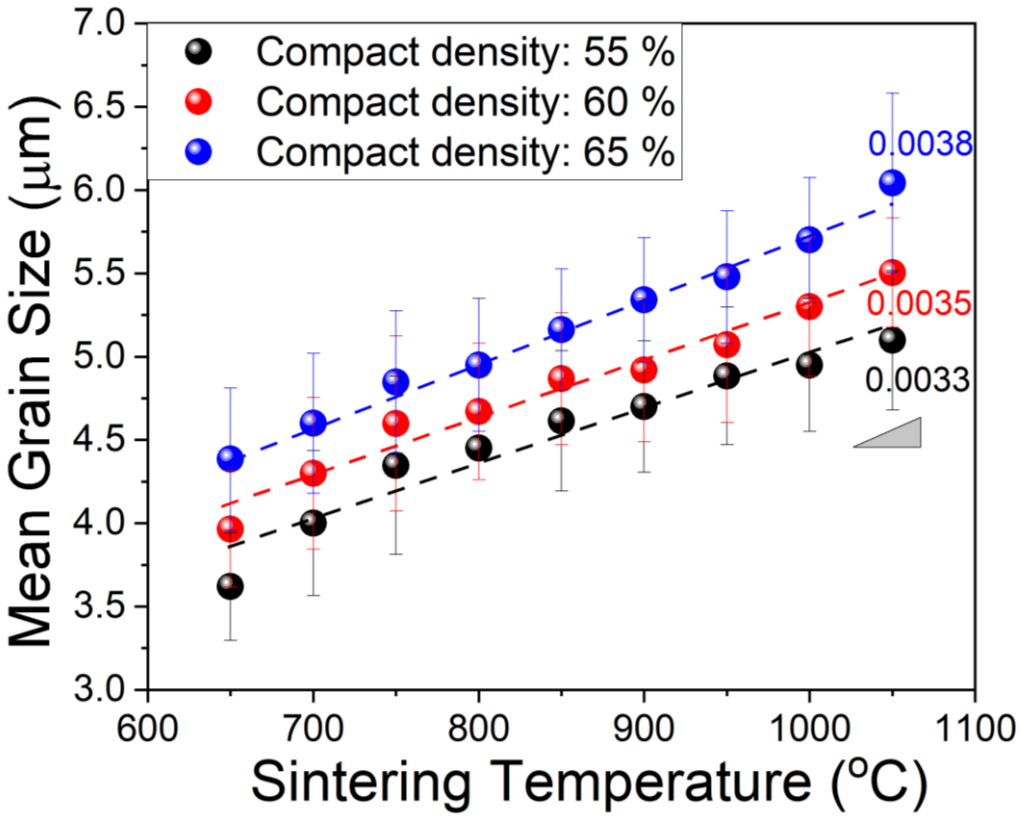


Figure 6. Relationship between mean grain size and sintering temperature as a function of the compact density. The dotted line represents the standard deviation of the mean grain size.

The classical grain growth kinetics [31–33] can be expressed as follows:

$$G_t^n - G_0^n = Kt \tag{5}$$

where G_t is the grain size at a given time, G_0 is the initial grain size, n is the grain growth exponent, K is a constant, and t is the sintering time. The variable n represents the grain growth behavior, and its value can be divided by the diffusion mechanism on the pore control as follows: 2 for vapor transport, 3 for vapor transport and lattice diffusion, and 4 for surface diffusion. The n value, even if a constant value is observed over a wide temperature and grain size range, does not indicate a specific mechanism; however, a value of 3 is most commonly observed [34]. The activation energy (Q, kJ/mol) for grain growth within the sintered MoO_2 samples with different compact densities was calculated according to the Arrhenius behavior [35]:

$$K = K_0 \exp\left(-\frac{Q}{RT}\right) \tag{6}$$

where K_0 is a constant, R is the gas constant (=8.314 J/(mol·K)), and T is the absolute temperature. The activation energy Q is the log of both sides of Equation (5) and can be expressed as

$$\ln\left(G_t^3 - G_0^3\right) = \ln K_0 + \ln t - Q/RT \quad (7)$$

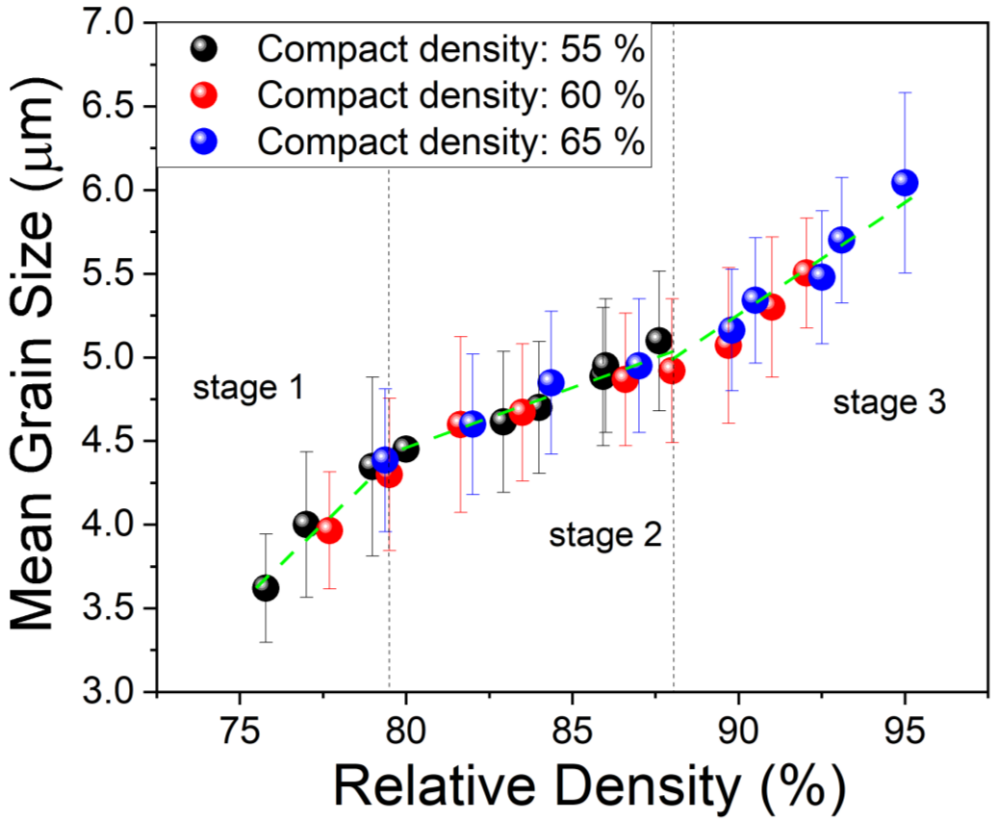


Figure 7. Grain growth behavior as a function of relative density. The dotted line represents the standard deviation of the mean grain size.

Equation (7) indicates that ln$G$ and $1/T$ show a linear relationship at the same sintering time, as shown in Figure 8, and the slope indicates the activation energy for grain growth. The calculated values of activation energy for the grain growth according to Equation (7) are summarized in Table 1, along with the reliability of the fit in the selected temperature ranges for different compact densities. A close examination of the graph reveals a linear relationship between the ln values of the y-axis and temperature for sintering temperatures below 750 °C, while a slight non-linearity is observed at higher temperatures. Linear fitting of individual data points yields R-squared values exceeding 0.996 for lower sintering temperatures, indicating a strong linear correlation. For sintering temperatures above 750 °C, the R-squared value decreases slightly to around 0.968. Nevertheless, given the high R-squared values obtained even at higher temperatures, the activation energy was calculated using Equation (7). Interestingly, the slopes for the samples with the compact density values within 55–60% were changed; however, the slope values for the sample with a compact density of 65% were a little varied at the sintering temperature of 750 °C indicated by the dotted line in Figure 8. This indicates that the dominant diffusion mechanism differed depending on the temperature of the loose compact samples. Below the sintering temperature of 750 °C, the slope values dramatically decreased with an increase in the compact density, indicating that the activation energy for grain growth decreases when the MoO_2 samples were denser at lower sintering temperatures. The results showed a decline in the activation energy in the sample with a high compact density, suggesting that more than one grain growth mechanism is operative in previously reported sintering experiments [36,37]. The

decreasing trend in activation energies is reasonable for deducing that volume diffusion is the dominant grain growth mechanism as a function of the compact density. Therefore, atom diffusion for the samples with low compact densities was more difficult for those with high compact densities because of the long distance between particles at the beginning of sintering. As a result, higher activation energy for grain growth reflects the increased difficulty of facilitating the diffusion process. Above this temperature, the slope increased slightly with an increase in the compact density. According to the sintering theory, grain boundary diffusion and lattice diffusion mechanisms simultaneously exist during the sintering of polycrystalline ceramics, and these mechanisms can be operated according to the temperature owing to their different temperature dependences. The relative contributions of lattice and grain boundary diffusion are different at different temperatures. As shown in Figures 6 and 7, the relative density plays a crucial role in non-isothermal sintering kinetics. By influencing the relative contributions of diffusion mechanisms, such as grain boundary diffusion and lattice diffusion, at elevated temperatures, it can significantly affect the overall sintering rate and final microstructure. The increase in the activation energy for grain growth above a high relative density could be explained by a larger relative contribution of lattice diffusion as compared to grain boundary diffusion because the grain boundary diffusion mechanism has a lower activation energy than lattice diffusion does. The classical grain boundary diffusion mechanism assumes that grain boundaries act as perfect sources and sinks for diffusing atoms during the diffusion process, thereby having a low activation energy owing to the provision of a tunnel for diffusion and exhibiting more activity [38].

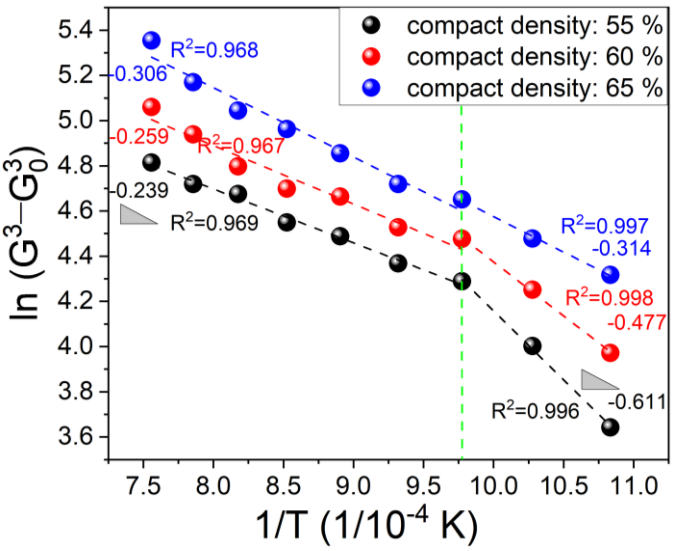


Figure 8. Arrhenius plot of the grain growth.

Table 1. Activation energies for grain growth during sintering process calculated from Figure 6.

Compact Density of Samples	Activation Energy (kJ/mol)	
	650–750 °C	750–1050 °C
55%	50.80	19.87
60%	39.66	21.53
65%	26.11	25.44

4. Conclusions

This study investigated the densification kinetics and grain growth of MoO_2 ceramic samples having different compact densities synthesized via pressureless sintering within a temperature range of 650 to 1050 °C for the same dwell time. The following conclusions were drawn from this study:

(1) MoO_2 remained phase-stable under N_2 atmosphere at 650–1050 °C. Densification of binderless MoO_2 compacts increased with initial density, attributed to enhanced interfacial contact and diffusion mechanisms facilitated by higher coordination numbers.
(2) Grain growth increases with compact density as particle rearrangement improves homogeneity. Higher densities activate capillary forces and surface diffusion, leading to coarsening and larger grains at elevated sintering temperatures.
(3) Using the Arrhenius theory, it was found that the activation energies for grain growth increase at low temperatures and decrease at high temperatures with a decrease in compact density. This is because atomic diffusion is difficult owing to the long distance between particles at the beginning of sintering. During immediate sintering, both the lattice and grain boundary diffusion mechanisms are dominant, and this can be attributed to the difference in the relative contribution of the lattice and grain boundary diffusion mechanisms to grain growth. From the results, the enhancement of interconnected particles is required to achieve fuller density.

Author Contributions: Conceptualization, J.L. and J.J.; methodology, J.J. and H.J.; software, J.L.; validation, J.L.; formal analysis, J.J.; investigation, J.J.; resources, H.L. and J.P.; data curation, J.J. and H.J.; writing—original draft preparation, J.L.; writing—review and editing, H.L. and J.P.; supervision, H.L.; project administration, J.P.; funding acquisition, J.P. All authors have read and agreed to the published version of the manuscript.

Funding: This research was funded by the Ministry of Trade, Industry and Energy, Korea; grant number 20022463 and 20016519.

Data Availability Statement: Data are contained within this article.

Conflicts of Interest: Authors Hyowon Lee and Jaesoung Park are employed by the company LT Metal. Co., Ltd. The remaining authors declare that the research was conducted in the absence of any commercial or financial relationships that could be construed as a potential conflict of interest.

References

1. Rahaman, M. *Ceramic Processing and Sintering*; Taylor & Francis: New York, NY, USA, 2003; pp. 425–619.
2. Wang, D.; Wang, X.; Xu, C.; Fu, Z.; Zhang, J. Densification mechanism of the ultra-fast sintering dense alumina. *AIP Adv.* **2020**, *10*, 025223. [CrossRef]
3. Campbell, C.; Parker, S.; Starr, D. The effect of size-dependent nanoparticle energetics on catalyst sintering. *Science* **2002**, *298*, 811–814. [CrossRef] [PubMed]
4. Messing, G.; Stevenson, A. Toward pore-free ceramics. *Science* **2008**, *322*, 383–384. [CrossRef] [PubMed]
5. Spusta, T.; Svoboda, J.; Maca, K. Study of pore closure during pressure-less sintering of advanced oxide ceramics. *Acta Mater.* **2016**, *115*, 347–353. [CrossRef]
6. Niesz, D. A Review of Ceramic Powder Compaction. *KONA Powder Part. J.* **1996**, *14*, 44–51. [CrossRef]
7. Shaw, N. Densification and coarsening during solid state sintering of ceramics: A review of the models. Pt. 1. Densification. *Powder Metall. Int.* **1989**, *21*, 16–21. Available online: https://www.osti.gov/etdeweb/biblio/5948159 (accessed on 1 October 1989).
8. Kingery, W.; Bowen, H.; Uhlmann, D.M. *Introduction to Ceramics*; John Wiley & Sons: New York, NY, USA, 1960.
9. Pan, J.; Cocks, A. A constitutive model for stage 2 sintering of fine grained materials-II Effects of an interface reaction. *Acta Metall. Mater.* **1994**, *42*, 1223–1230. [CrossRef]
10. Wang, S.; Guo, H.; Song, Y.; Ma, G.; Li, S.; Zhang, L.; Shao, X. P-63: Lower Reflective TFT Materials and Technology Innovation. *SID Symp. Dig. Tech. Pap.* **2017**, *48*, 1478–1481. [CrossRef]
11. Pachlhofer, J.; Martín-Luengo, A.; Franz, R.; Franzke, E.; Köstenbauer, H.; Winkler, J.; Bonanni, A.; Mitterer, C. Industrial-scale sputter deposition of molybdenum oxide thin films: Microstructure evolution and properties. *J. Vac. Sci. Technol.* **2017**, *35*, 021504. [CrossRef]
12. Reza, M.; Sajuri, Z.; Yunas, J. Effect of sputtering target's grain size on the sputtering yield, particle size and coercivity (Hc) of Ni and Ni20Al thin films. *IOP Conf. Ser.* **2020**, *778*, 012116. [CrossRef]
13. Lee, J.; Jeong, J.; Lee, H.; Park, J.; Jang, J.; Jeong, H. Effects of Sintering Processes on Microstructure Evolution, Crystallite, and Grain Growth of MoO_2 Powder. *Crystals* **2023**, *13*, 1311. [CrossRef]
14. Xiang, H.; Xing, Y.; Dai, F.; Wang, H.; Su, L.; Miao, L.; Zhang, G.; Wang, Y.; Qi, X.; Yao, L.; et al. High-entropy ceramics: Present status, challenges, and a look forward. *J. Adv. Ceram.* **2021**, *10*, 385–441. [CrossRef]
15. Zhang, W.; Chena, L.; Xu, C.; Lv, X.; Wang, Y.; Ouyang, J.; Zhou, Y. Grain growth kinetics and densification mechanism of (TiZrHfVNbTa)C high-entropy ceramic under pressureless sintering. *J. Mater. Sci. Technol.* **2022**, *110*, 57–64. [CrossRef]

16. Bolzan, A.; Kennedy, B.; Howard, C. Neutron powder diffraction study of molybdenum and tungsten dioxides. *Aust. J. Chem.* **1995**, *48*, 1473–1477. [CrossRef]
17. Mendelson, M. Average Grain Size in Polycrystalline Ceramics. *J. Am. Ceram. Soc.* **1969**, *52*, 443–446. [CrossRef]
18. Yi, H.; Pandeya, A.; Karamchandani, A.; Puri, V. Critical Review on Engineering Mechanical Quality of Green Compacts using Powder Properties. *KONA Powder Part. J.* **2018**, *35*, 32–48. [CrossRef]
19. Lawrence, P. Low Temperature Nanoscale Oxygen-Ion Intercalation into Epitaxial MoO2 Thin Films. *J. Phys. Chem. C.* **2017**, *121*, 3410–3415. [CrossRef]
20. Niesz, D.; Bennett, R.; Snyder, M. Strength characterization of powder aggregates. *Am. Ceram. Soc. Bull.* **1972**, *51*, 677–680. [CrossRef]
21. Diantonio, C.; Ewsuk, K.; Bencoe, D. Extension of Master Sintering Curve Theory to Organic Decomposition. *J. Am. Ceram. Soc.* **2005**, *10*, 2722–2728. [CrossRef]
22. Rajeswari, K.; Padhi, S.; Reddy, A.; Johnson, R.; Das, D. Studies on sintering kinetics and correlation with the sinterability of 8Y zirconia ceramics based on the dilatometric shrinkage curves. *Ceram. Int.* **2013**, *39*, 4985–4990. [CrossRef]
23. Aman, Y.; Garnier, V.; Djuradoy, E. Spark plasma sintering kinetics of pure α-alumina. *J. Am. Ceram. Soc.* **2011**, *94*, 2825–2833. [CrossRef]
24. Chen, P.; Chen, W. Sintering Fine Oxide Powders: I, Microstructural Evolution. *J. Am. Ceram. Soc.* **1996**, *79*, 3129–3149. [CrossRef]
25. Dehoff, R. *A Cell Model for Microstructural Evolution During Sintering: Sintering and Heterogeneous Catalysis*; Plenum Press: New York, NY, USA, 1984; pp. 471–496.
26. Kang, S. *Sintering: Densification, Grain Growth and Microstructure*; Elsevier Butterworth-Heinemann: Oxford, UK, 2005. Available online: https://books.google.co.kr/books?id=uPWbuZohRmoC&printsec=frontcover&redir_esc=y#v=onepage&q&f=false (accessed on 2 February 2005).
27. Greskovich, C.; Lay, K. Grain Growth in Very Porous Al2O3 Compacts. *J. Am. Ceram. Soc.* **1972**, *55*, 142–146. [CrossRef]
28. Exner, H.; Muller, C. Particle rearrangement and pore space coarsening during solid state sintering. *J. Am. Ceram. Soc.* **2009**, *92*, 1384–1390. [CrossRef]
29. He, Z.; Ma, J. Densification and grain growth during interface reaction controlled sintering of alumina ceramics. *Ceram. Int.* **2001**, *27*, 261–264. [CrossRef]
30. Bregiroux, D.; Audubert, F.; Dernache-assollant, D. Densification and grain growth during solid state sintering of LaPO4. *Ceram. Int.* **2009**, *35*, 1115–1120. [CrossRef]
31. Gleiter, H. Nanocrystalline materials. *Prog. Mater. Sci.* **1989**, *33*, 223–315. [CrossRef]
32. Lu, K. Nanocrystalline metals crystallized from amorphous solids: Nanocrystallization, structure, and properties. *Mater. Sci. Eng. R Rep.* **1996**, *16*, 161–221. [CrossRef]
33. Gil, F.; Picas, J.; Manero, J.; Forn, A.; Planell, J. Effect of the addition of palladium on grain growth kinetics of pure titanium. *J. Alloys Compd.* **1976**, *260*, 147–152. [CrossRef]
34. Wang, F. *Ceramic Fabrication Processes: Treatise on Materials Science and Technology*; Academic Press Inc.: Orlando, FL, USA, 1976; p. 9.
35. Milsom, B.; Porwal, H.; Viola, G.; Gao, Z.; Reece, M. Understanding and quantification of grain growth mechanism in ZrO_2-carbon nanotube composites. *Mater. Des.* **2017**, *133*, 325–331. [CrossRef]
36. Liu, Z.; Loh, N.; Khor, K.; Tor, S. Sintering activation energy of powder injection molded 316L stainless steel. *Scr. Mater.* **2001**, *44*, 1131–1137. [CrossRef]
37. Bernard-granger, G.; Guizard, C. Apparent Activation Energy for the Densification of a Commercially Available Granulated Zirconia Powder. *J. Am. Ceram. Soc.* **2007**, *90*, 1246–1250. [CrossRef]
38. Shao, W.; Chen, S.; Li, D.; Cao, H.; Zhang, Y.; Zhang, S. Apparent activation energy for densification of α-Al_2O_3 powder at constant heating-rate sintering. *Bull. Mater. Sci.* **2008**, *31*, 903–906. [CrossRef]

Disclaimer/Publisher's Note: The statements, opinions and data contained in all publications are solely those of the individual author(s) and contributor(s) and not of MDPI and/or the editor(s). MDPI and/or the editor(s) disclaim responsibility for any injury to people or property resulting from any ideas, methods, instructions or products referred to in the content.